

Investigation of the Mixing Process in an Axisymmetric Turbulent Jet Using PIV and LIF

by

C. Fukushima, L. Aanen, J. Westerweel

Laboratory for Aero and Hydrodynamics
Delft University of Technology

Rotterdamseweg 145, 2628 AL Delft, The Netherlands

ABSTRACT

In the present paper, mixing of a passive scalar in a self-preserving axisymmetric turbulent jet at a Reynolds number of 2×10^3 is studied utilizing combined particle image velocimetry (PIV) and planar laser induced fluorescence (LIF). Detailed measurements are made for the mean velocity, turbulent intensity of velocity fluctuation, Reynolds shear stress, mean concentration, concentration fluctuation intensity, and turbulent flux at the center plane of the jet. In order to examine the reliability of the results, mass balances that are based on the mass-balance equation are also estimated. These results will be a reference data set for further investigation of the chemically reacting turbulent jet. The results are compared with the results from direct numerical simulation, point velocity measurements, and combined PIV, particle tracking velocimetry (PTV), or laser Doppler velocimetry (LDV) and LIF measurements. All the properties collapse onto self-similar profiles in the far field (30-60 diameter downstream from the nozzle) of the jet, and agree with the previous data. In the case of the present data, the mass balances are conserved quite well.

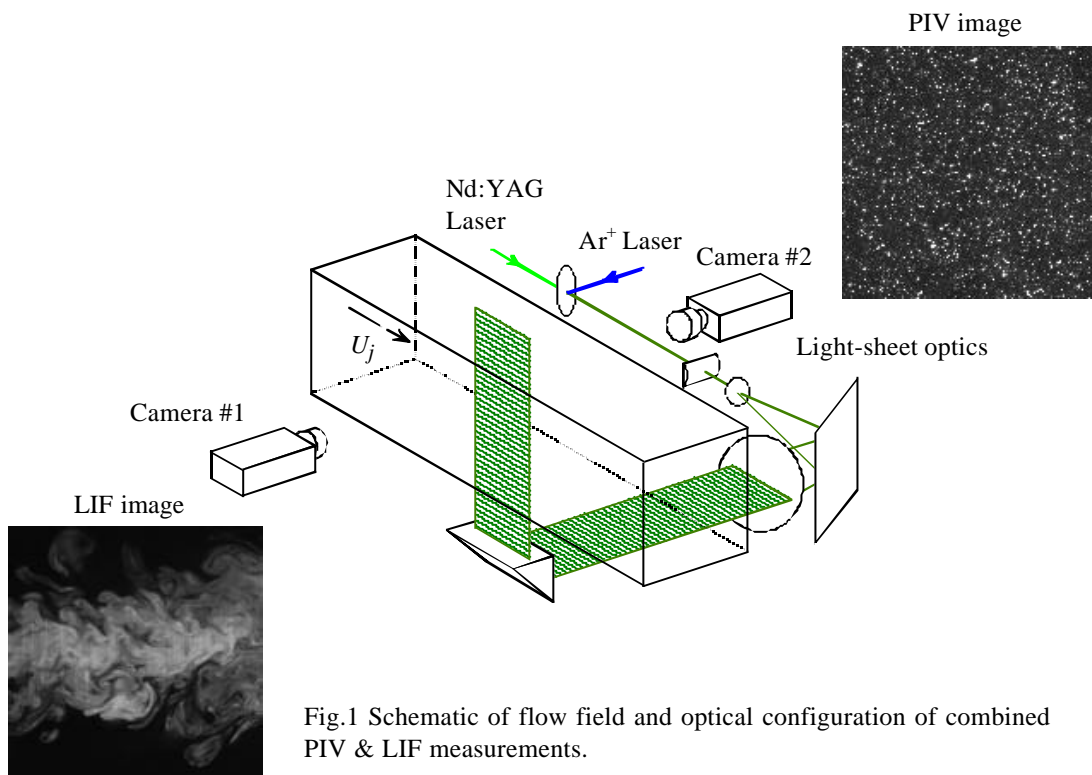


Fig.1 Schematic of flow field and optical configuration of combined PIV & LIF measurements.

1. INTRODUCTION

Turbulent jet flow has been widely studied for its mixing properties. Mixing of passive scalars, such as heat or contaminants, is one of the significant features of the turbulence, and the jet flow in combination with turbulent mixing and the chemical reaction can be found in many practical applications (e.g. fuel injectors in combustion engines). In order to improve the efficiency of such devices, it is important to obtain more insight into turbulent mixing. In the experimental investigation of turbulent mixing, it is necessary to measure the instantaneous velocity and concentration field, simultaneously, since the mixing process can be described as the interaction between a velocity and concentration field.

In the present study, we investigated the mixing of a passive scalar contaminant in a turbulent free jet with a surrounding fluid. The Reynolds averaged equation for the conservation of the mean concentration of a passive scalar in an axisymmetric jet is given by,

$$U \frac{\partial C}{\partial z} + V \frac{\partial C}{\partial r} = D \left[\frac{\partial^2 C}{\partial z^2} + \frac{1}{r} \frac{\partial}{\partial r} \left(r \frac{\partial C}{\partial r} \right) \right] - \frac{\partial}{\partial z} \overline{uc} - \frac{1}{r} \frac{\partial}{\partial r} (r \overline{vc}) \quad (1)$$

where U , V and C are the mean axial and radial velocity and the mean concentration respectively, z and r are the axial and radial coordinate respectively, D is the molecular diffusion coefficient, and \overline{uc} and \overline{vc} are the correlation of the axial and radial velocity fluctuation and the concentration fluctuations respectively. The terms on the left hand side of (1) are the advection of the mean concentration by the mean flow. The first term on the right hand side represents the molecular diffusion. The remaining terms on the right hand side represent the transport of the passive scalar by the turbulence.

Of particular interest to the present study are the radial and axial turbulent fluxes of the passive scalar. Therefore, these simultaneous measurements were achieved by utilizing combined particle image velocimetry (PIV) and planar laser induced fluorescence (LIF). The combined PIV and LIF measurement system is already developed in our laboratory and applied for the mixing of a point source placed at the centerline of a fully developed turbulent pipe flow (Aanen et al. 1999).

The aim of the present study is to obtain a reliable reference data set for the further investigation of chemically reacting turbulent jets. Detailed measurements are made for the mean and fluctuating velocity, mean concentration, concentration fluctuation intensity, and turbulent flux. In order to validate the present data set, the results are compared with the results of a direct numerical simulation (Boersma et al. 1998, Lubbers et al. 2000), various point velocity measurement (Panchapakesan & Lumley 1993, Wagnanski & Fiedler 1969), and with the results of measurements with combined PIV/LIF (Law & Wang 1998), PTV/LIF (Webster et al. 2000) or LDV/LIF (Papanicolaou & List 1988). Additionally, the mass balance in equation (1) is examined in detail.

2. MEASUREMENT TECHNIQUES

Particle image velocimetry (PIV) is used to measure the instantaneous velocity field in a planar cross section of the observed flow. With PIV, the fluid velocity is determined by measuring the displacement of small tracer particles, over a small time interval. The tracer particles are illuminated by a thin light sheet, which exposes the tracer particles two times, with a small time delay. The light scattered from the tracer particles is recorded with a CCD camera, where each exposure is recorded in a separate frame. The displacement of the particles is determined by computing the spatial cross-correlation in small interrogation windows of each frame pair. Sub-pixel displacements are estimated by means of a Gaussian peak fit to the correlation peak for both the horizontal and vertical components of the displacement (Westerweel 1993). The estimated precision for the measured displacement by the method is 0.05-0.10 pixel units.

The instantaneous concentration distribution in a planar cross section of the flow is measured with laser induced fluorescence (LIF). The concentration of a fluorescent dye is observed by measuring the amount of light emitted by the dye when it is illuminated by a light source with a known intensity distribution. The light that is absorbed by the dye is emitted at a longer wavelength, and the intensity of the emitted light is directly proportional to the local concentration of the dye. The instantaneous planar distribution of the emitted light is measured with a CCD camera. For the calibration, the measurement

section is filled with a uniform dye concentration and a series of 100 images are recorded and then averaged at each pixel. Besides that, a series of 50 dark images are recorded after each measurement to determine the gray value offset for each pixel. The difference of these two yields the local light intensity distribution. The concentration distributions are determined by subtracting the gray offset value distribution, and then normalizing with the light intensity distribution.

Detailed descriptions of PIV are given by Adrian (1991) and Westerweel (1993), and of LIF by Walker (1987) and Koochesfahani (1984).

3. EXPERIMENTAL CONFIGURATION

The measurements are carried out in a rectangular test section ($110 \times 110 \times 300 \text{ mm}^3$) fitted in a closed-loop water pipe facility with a total length of 6 m. A schematic of the experimental configuration is shown in Fig.1. The jet is discharged by driving an electromotor which drives a syringe, and injected through a long thin needle with an inner diameter d of 1 mm. A fluorescent dye (fluorescein) is used as a scalar, so that the Schmidt number S_c (i.e. the ratio of kinematic viscosity to molecular diffusivity) of the dye is 2075. This implies that the molecular diffusion term in equation (1) is negligible with respect to the turbulent diffusion. The self-preserving axisymmetric turbulent jet is then obtained in the test section some distance downstream of the nozzle. All the measurements are made in a plane through the centerline of the jet in the region of $z/d = 20-140$ at a Reynolds number $Re (=U_j d/\nu) = 2 \times 10^3$. This value was chosen to match the Re -number of a DNS by Boersma et al. (1998).

A combined PIV and LIF measurement system is already developed in our laboratory (Aanen et al. 1999). For the illumination of the PIV image and light source of the LIF measurements, a twin Nd:YAG pulsed laser (wavelength of 532 nm, 200 mJ per pulse) and a CW Argon-ion laser (wavelength of 488 nm, 2.4 W) are used respectively. Both the laser beams are combined along the same optical path and transformed into a light sheet (see Fig.1). The light sheet has a thickness of less than 1 mm over a length of 50 mm, and is almost parallel across the test section with a width of 50 mm. The light intensity scattered by the particles and the light intensity of the fluorescent dye are recorded separately on two synchronized digital CCD cameras (Kodak ES-1.0, 992×1004 pixels). The observed common area is about $45 \times 45 \text{ mm}^2$ using 55 mm micro Nikkor lenses. The alignment between these cameras is accurate within 3 pixels, i.e. less than 0.3% of the image dimension.

Both the PIV and LIF measurements do not influence each other by using a shutter and appropriate optical low-pass filters. In order to completely avoid mutual influence of the measurements, PIV and LIF measurements are made sequentially. In the present case, the time delay between the two laser pulses are 0.24, 1.2, and 2.4 ms at each streamwise section with center positions of the camera at $z/d = 40, 80$ and 120 respectively for PIV, so the particle-image displacement is about one-quarter of the interrogation domain. The exposure times are 0.9, 2.4, and 4.8 ms respectively for LIF. These times are a compromise between an exposure that is long enough to record an adequate image and short enough to avoid motion blurring of the image. The total duration of the measurement is 1.5-7.6 ms, which is shorter than the Kolmogorov time scale, so it is considered that the combined PIV and LIF measurements are made simultaneously. A sample image of each PIV and LIF measurement is also shown in Fig. 1.

The signals from the cameras are digitized and recorded by two pipeline processors (Datacube MV-200), and then a continuous image sequence of 134 frames is obtained at a rate of 15 Hz with double trigger mode. For each measurement location, 12 sequences of images are recorded so that one measurement includes 804 frame pairs that cover a total measurement time of 53.6 sec.

4. RESULTS AND DISCUSSION

4.1 Mean Velocity and Turbulent Statistics

All the results are obtained at 3 positions in the streamwise section including 61×61 statistics at each position. The total of three positions correspond to a downstream distance in the z/d range of 20-140 with an axial and radial spacing of 0.75. However, in the initial mixing region the fluorescent dye and tracer particles are not yet well mixed, so that reliable data are obtained in the z/d range from 30 for the velocity field.

Figure 2 shows the decay of the mean centerline velocity and concentration as a function of the distance from the nozzle respectively. Each peak value is obtained from the least-square fit of Gaussian function, or parabolic function, to the mean velocity and concentration profile, and is recognized as the centerline value. The results for the mean velocity and the mean concentration clearly show the z^{-1} decay of the jet. The virtual origin of the velocity and concentration fields are 6.75 and 6.76 mm respectively. The value of $z_0 = 6.75d$ for the velocity field is slightly larger than the result of DNS (Boersma et al. 1998), which is $z_0 = 4.9d$, and that of the measurement (Wyganski & Fiedler 1969), $z_0 = 3-7d$, since the virtual origin significantly depends on the Reynolds number and the initial condition of the jet.

The streamwise development of the half width for the velocity b_u and the scalar b_c are shown in Fig.3. It is important to examine the development of the length scale in detail, since the present jet is not

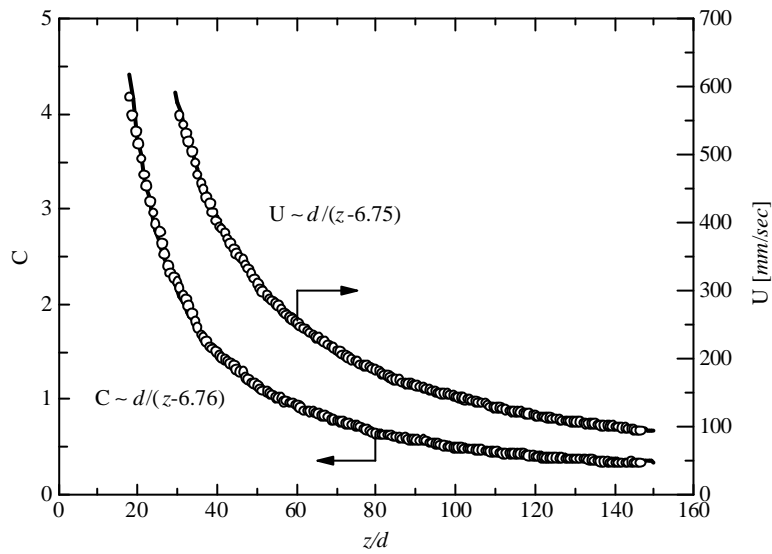


Fig.2 Variation of the centerline mean velocity and mean concentration along the jet axis.

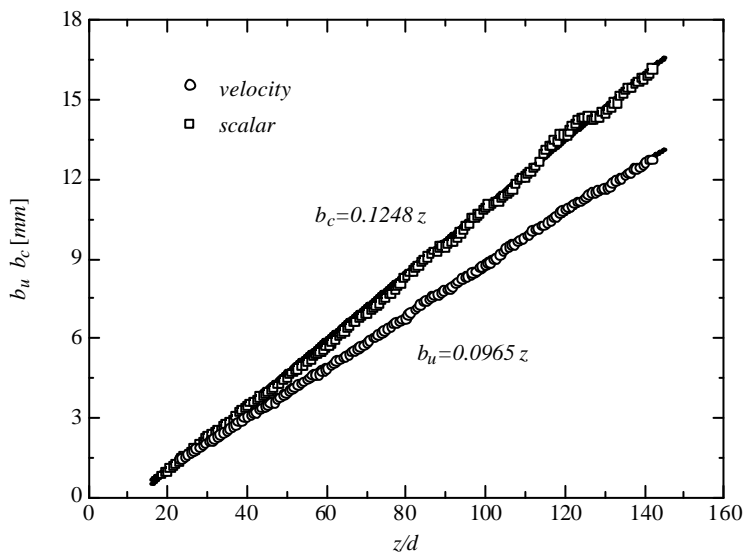


Fig.3 Streamwise development of the half width for the velocity field and concentration field.

an ideal free jet in the far downstream region, due to the wall boundary of the test section. The results show the linear development of the length scale, where $b_u = 0.097z$ and $b_c = 0.125z$ respectively, and there is no wall constraint effect on the jet development within the present experimental extent. Each coefficient 0.097 and 0.125 agree with the average of previous results (Fischer et al. 1979). Therefore it can be expected that self-preserving turbulent jets are established in the present experiment.

The axial mean velocity for the 12 representative streamwise sections are shown in Fig.4. The axial mean velocity U , which is normalized by the centerline velocity U_c , is plotted versus the non-dimensional radial coordinate, $\eta = r/(z-z_0)$. All the profiles collapse onto a single profile within the experimental extent. When the profiles are examined in detail, a small reverse flow (i.e., a negative value of U) is observed in the region $|\eta| > 0.2$ in the far downstream region. If the velocity profile is assumed Gaussian it becomes $U/U_c = \exp(-K_u \eta^2)$. The average of the least-square fit to all the data gives $K_u = 84.9$,

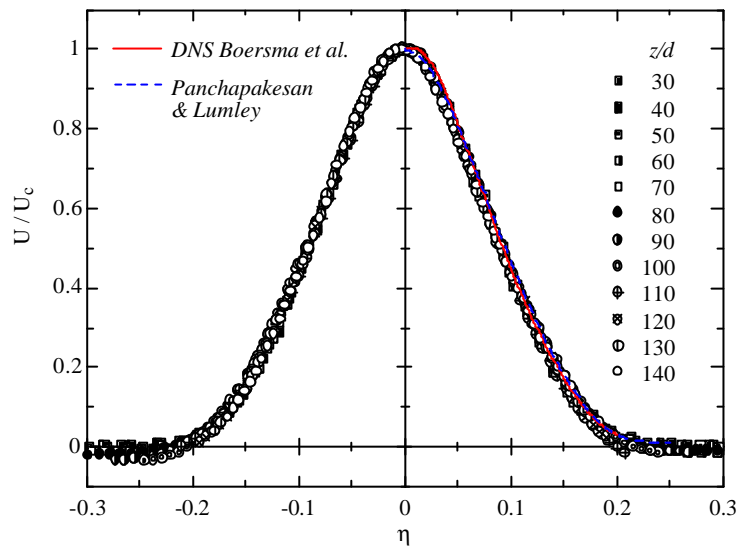


Fig.4 Axial mean velocity profile across the jet.

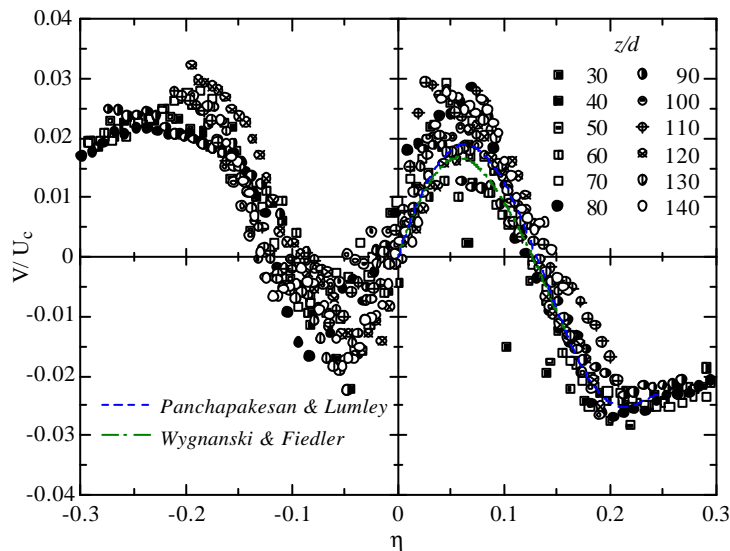


Fig.5 Radial mean velocity profile across the jet.

whereas in the experiment by Panchapakesan & Lumley (1993) a value of 75.2 (at a Reynolds number of 1.1×10^4) and in the DNS by Boersma et al. (1998) a value of 76.1 (at a Reynolds number of 2.4×10^3) have been found respectively. It means that the spread of the center region of the profile is slightly narrower than other results. Although, there is a slight effect on the velocity profile due to the wall constraint of the test section in the far downstream region, the profiles can be considered self-similar within the experimental extent.

Figure 5 shows the radial mean velocity profile at each representative streamwise section. The results in Panchapakesan & Lumley (1993) and Wagnanski & Fiedler (1969) are obtained from the curve fit of the axial velocity and the continuity equation. The present results exhibit a relatively high scatter due to the small absolute value of the V to the PIV resolution, however the averaged peak value throughout the data, and the distributions of the velocity profile agree well with the previous estimation.

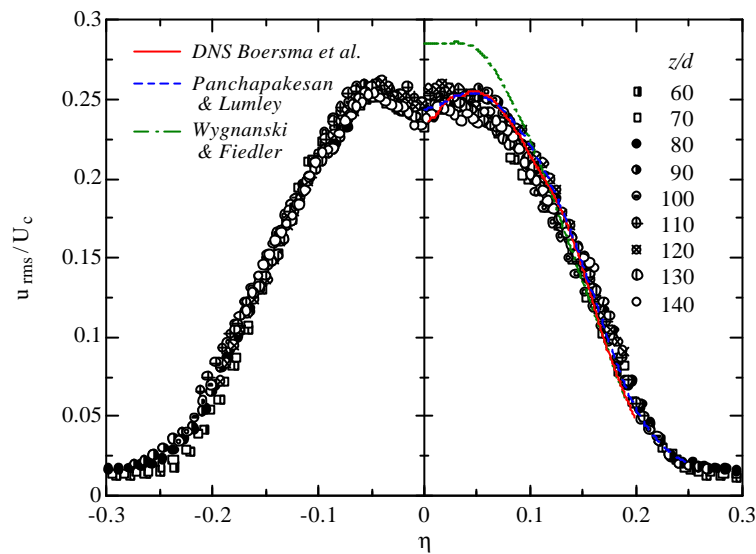


Fig.6 Turbulent intensity of the axial velocity fluctuations across the jet.

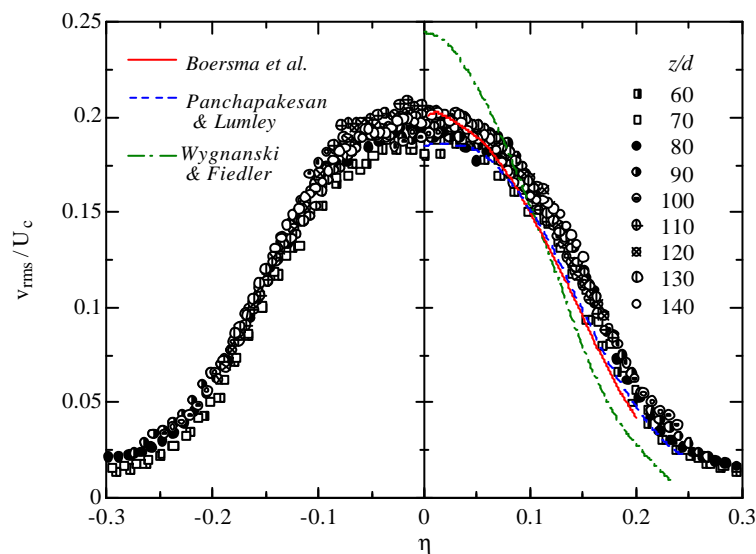


Fig.7 Turbulent intensity of the radial velocity fluctuations across the jet.

The radial profiles of the turbulent intensity of the axial and radial velocity component are shown in Fig. 6 and Fig. 7 respectively. There is a distinct off-axis peak in the profile of the axial velocity fluctuations, which is also seen in the DNS results (Boersma et al. 1998) and the experimental results of Panchapakesan & Lumley (1993). This peak is expected from the profile of shear production of the kinematic energy, which has a distinct peak at nearly same location. The value at the centerline, the off-axis peak value and the location of the peak agrees well with the results of DNS and Panchapakesan & Lumley. For the radial velocity fluctuations, the present results almost agree with the DNS results of Boersma et al. (1998) near the centerline. The results from Wygnanski & Fiedler (1969) have quite higher peak values (Figs. 6 and 7) and the profile is narrower (Fig.7) than the present or other results. This is probably due to the effect of the confinement of the jet, where the momentum loss arises due to the reverse flow, as suggested by Panchapakesan & Lumley (1993). In the present results, therefore, each turbulent intensity profile has reached its self-similar state in the region of $z/d \geq 60$. In the range of $z/d = 30-50$ (not shown here) the profiles have a relatively lower peak value at the center and higher value around the outer edge. As one of the reasons of such results, it may be supposed that the time delay between two laser pulses is adjusted for the nearest position from the nozzle, so the results include experimental uncertainty of 13-25% around $z/d = 50$.

The Reynolds shear stress profiles for the 12 representative streamwise sections are shown in Fig.8. The Reynolds shear stress is asymmetric about the centerline, as expected; positive where the mean shear is negative, and negative where the mean shear is positive. In the present data, location of the peak value of the shear stress is 0.06-0.07, which agrees well with that of the radial component of mean velocity, and slightly larger than that of the turbulent intensity of 0.05. The sign of the shear stress corresponds to the transport of high momentum away from the centerline. The shear stress profiles almost agree with the results of DNS (Boersma et al. 1998) and Panchapakesan & Lumley (1993), while the result from Wygnanski & Fiedler (1969) has lower peak value and is narrower than our present measurements. Therefore, the Reynolds shear stress has reached its self-similar state in the region of $z/d \geq 60$.

4.2 Mean Concentration and Turbulent Flux

As shown in Fig.2 and Fig.3, the mean centerline concentration profiles collapse onto the curve proportional to z^{-1} . And the concentration field exhibit linear development, which is faster than the velocity field.

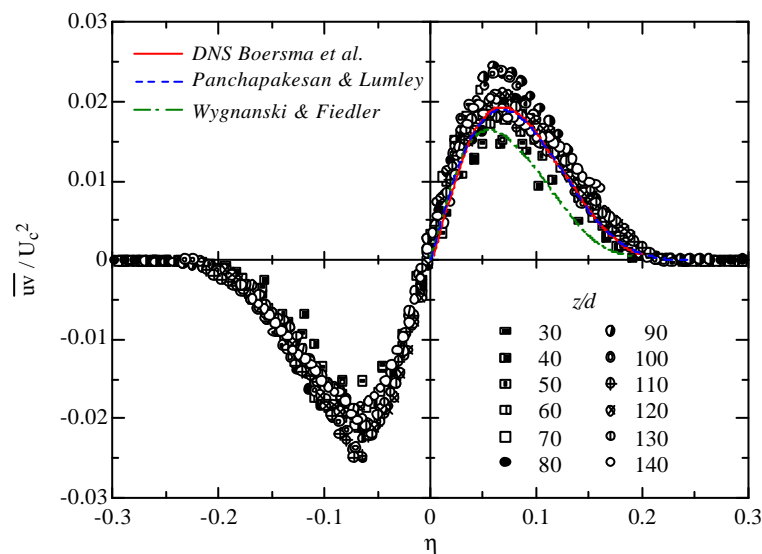


Fig.8 Reynolds shear stress variation across the jet

The radial profile of mean concentration across the center plane is shown in Fig.9. The mean concentration C , which is normalized by the centerline concentration C_c , is plotted versus the non-dimensional radial coordinate, $\mathbf{h} = r/(z-z_0)$. All the profiles collapse onto a single profile within the experimental extent. When the mean concentration profile is assumed as Gaussian, it becomes $C/C_c = \exp(-K_c \mathbf{h}^2)$. The average of the least-square fit to all the data gives $K_c = 56.9$, whereas in the DNS of Lubbers et al. (2000) at a Reynolds number of 2.0×10^3 a value of 59.1 was found. Although this means that the spread of the present profile is slightly wider than the DNS results, these K_c values seem in good agreement. Also the present data agrees well with the combined PTV (particle tracking velocimetry) and LIF measurements by Webster et al. (2000) at a Reynolds number of 3.0×10^3 . Therefore, the mean concentration is considered to be self-similar and independent of the Reynolds number. When the value

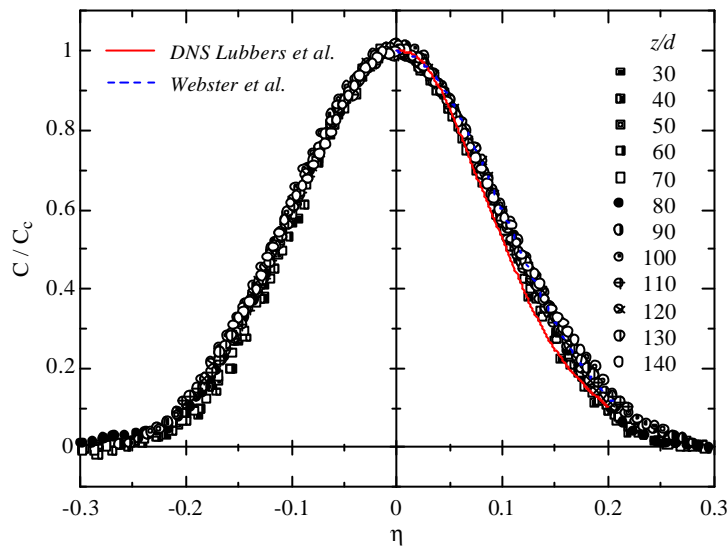


Fig.9 Mean concentration profile across the jet.

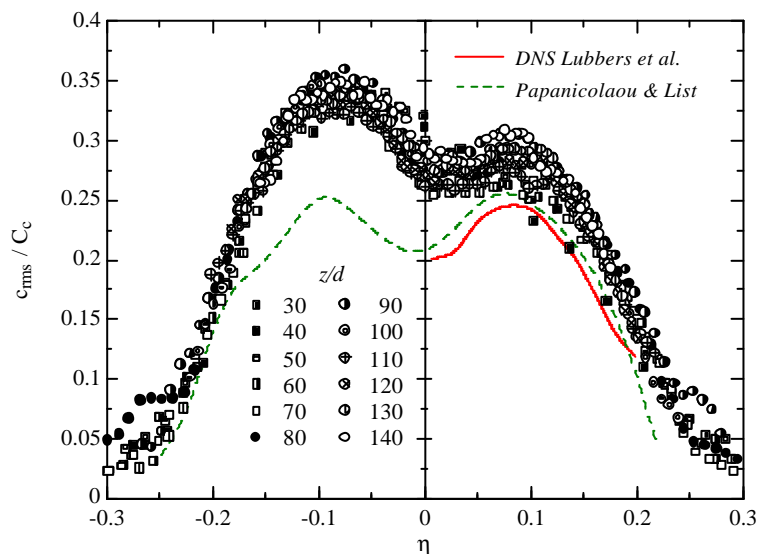


Fig.10 Concentration fluctuation intensity across the jet.

$K_c = 56.9$ is compared with $K_u = 84.9$, which is the value for the axial mean velocity, it is found that the concentration field spread faster than the velocity field as observed in Fig.2. This is associated with the preferential transport of the scalar over momentum as suggested by Lubbers et al. (2000).

The radial variation of concentration fluctuation intensity is shown in Fig.10. All the profiles at the representative streamwise section almost collapse onto a single profile. However, the profile is asymmetric about the centerline, and the peak value is significantly higher (especially negative h region) than DNS (Lubbers et al. 2000) and combined LDV/LIF measurement (Papanicolaou & List 1988). The negative region of the h correspond to the lower side of the test section. Therefore, there is a possibility of the effect of the absorption of the light due to the fluorescent dye. In the present measurements, any adjustment of the results is not applied.

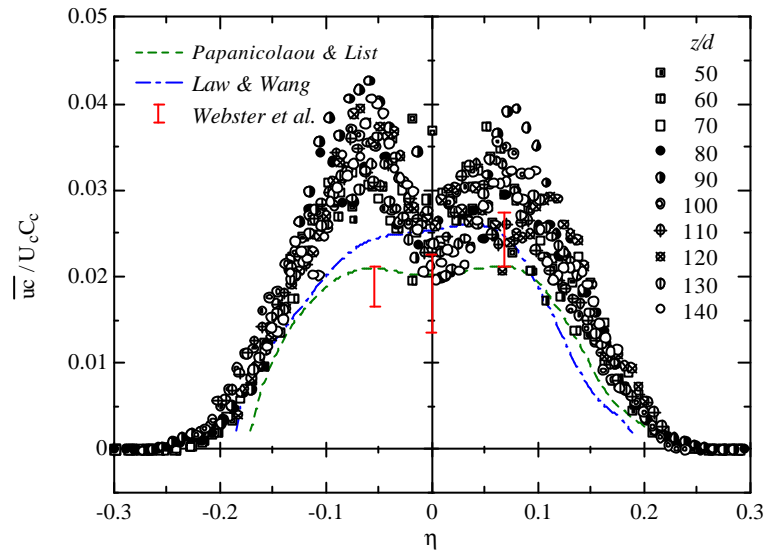


Fig.11 Axial turbulent flux \overline{uc} across the jet.

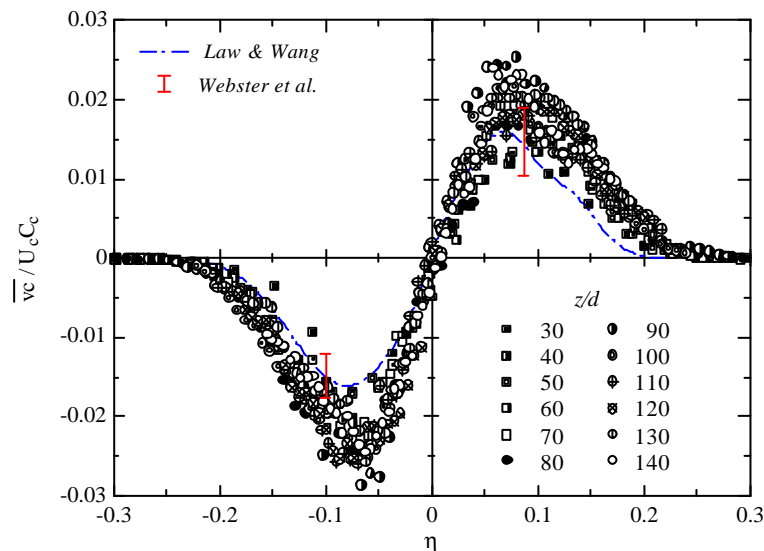


Fig.12 Radial turbulent flux \overline{vc} across the jet.

The axial and radial turbulent flux \overline{uc} and \overline{vc} are shown in Fig. 11 and Fig.12 respectively. The turbulent flux \overline{uc} and \overline{vc} are normalized by the mean centerline velocity and concentration. The curves in these figures are the curve-fits given by Papanicolaou & List (1988), and by Law & Wang (1998). These results show a similar scatter level with the results given by Webster et al. (2000). The axial turbulent flux collapse onto a single profile, and the exhibition of a significant off-axis peak which is also seen in the result of Papanicolaou & List. The position of the off-axis peak is about 0.07, which is slightly larger than that of turbulent intensity, and almost agrees with that of Reynolds shear stress and radial turbulent flux \overline{vc} . The averaged value at the centerline almost agrees with the result of Law & Wang, however, the value around the off-axis is significantly higher than other results. The radial profiles of the turbulent flux \overline{vc} show asymmetric profile about the centerline, as expected. The profiles collapse onto a single profile in the region from $z/d \geq 50$, and exhibit fewer scatter than observed in the axial turbulent flux. This is similar manner with the results of Webster et al. (2000). However, present results show slightly larger value of turbulent flux than those of Webster et al. and Law & Wang (1998). Boersma et al. (1998) pointed out that scaling of \overline{uv} , which is considering the growth rate of the half width, gives better results for the similarity profile of \overline{uv} . It means that the results could depend on the initial conditions of the jet. In fact there is a difference of the growth rate of the half width for the scalar between present data ($db_c/dz = 0.125$) and Webster et al. ($db_c/dz = 0.140$).

In order to assess the consistency of the present results, mass balances based on equation (1) are estimated. As mentioned above, molecular diffusion term is negligible since $S_c \gg 1$. In addition, variation of the turbulent flux in the axial direction is also negligible applying the boundary layer approximation, i.e. $|\partial \overline{uc} / \partial z| \ll |(1/r) \partial r \overline{vc} / \partial r|$. The results are shown in Fig.13 for 3 representative streamwise sections. The left hand side (closed symbols) of the equation (1) is slightly larger than right hand side (open symbols), which is observed most of the streamwise sections. This is probably due to the finite spatial resolution of the present measurements and the fact that the concentration fluctuations are highly intermittent. However, the difference between these terms is at an acceptable level.

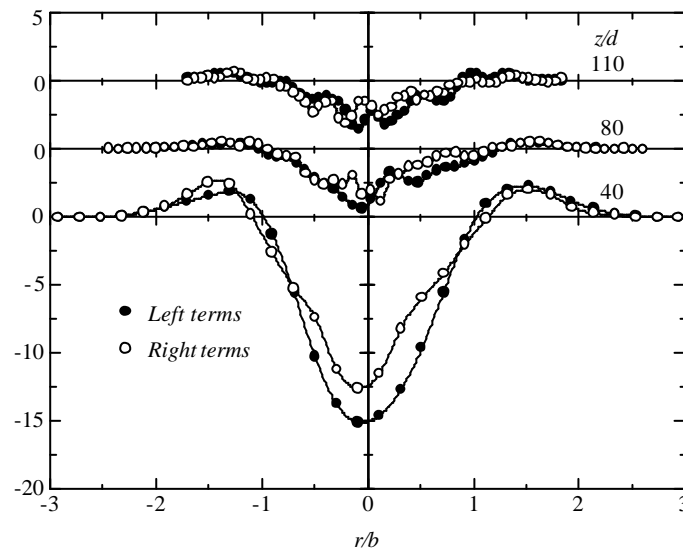


Fig.13 Estimation of the left and right hand side terms in the mass-balance equation.

5. CONCLUSIONS

In the present study, in order to obtain the reliable data set, detailed measurements were made for the mixing of a passive scalar in an axisymmetric turbulent free jet utilizing combined PIV and LIF method. The results were compared with the DNS, various point measurements and combined measurements. All the profiles of the mean velocity, turbulent intensity, Reynolds shear stress, mean concentration, concentration fluctuation intensity, and turbulent flux collapse onto each single profile. The results for the velocity field exhibit good agreement with the previous results, which is within the statistical sampling error. Although the discrepancy was not recognized in the mass-balance equation of the present measurements, some scatter especially in the axial turbulent flux and asymmetric profiles in the concentration fluctuation intensity, were observed. Therefore, it is necessary to increase the duration of the measurement, or to adjust the relation between the fluorescein concentration and exposure time.

The present results demonstrate the possibilities and the limitations of this combined PIV and LIF method for investigating turbulent mixing. We plan to continue this kind of investigation such as jet flow in combination with chemical reaction. In such an investigation, the local pH dependency of the fluorescent dye will be used to determine the influence of the turbulent mixing on the chemical reaction. Understanding of the turbulent mixing involving the chemical reaction is quite important for such as engineering design and environmental problems.

ACKNOWLEDGEMENT

The authors would like to thank Dr.ir. B.J. Boersma for his contributions to this project.

REFERENCES

- Aanen, L., Telesca, A. & Westerweel, J. 1999 Measurement of turbulent mixing using PIV and LIF. *Machine Vision & Graphics* **8**, 529-543.
- Adrian, R.J. 1991 Particle-imaging techniques for experimental fluid mechanics. *Annu. Rev. Fluid Mech.* **22**, 261-304.
- Boersma, B.J., Brethouwer, G. & Nieuwstadt, F.T.M. 1998 A numerical investigation on the effect of the inflow conditions on the self-similar region of a round jet. *Phys. Fluids* **10-4**, 899-909.
- Fischer, H.B., List, E.J., Koh, R.C.Y., Imberger, J. & Brooks, N.H. 1979 *Mixing in Inland and Coastal Waters*. Academic Press, New York.
- Koochesfahani, M.M. 1984 Experiments on turbulent mixing and chemical reactions in a liquid mixing layer. Ph.D.-Thesis California Institute of Technology, Pasadena.
- Law, A.W.-K. & Wang, H. 1998 Simultaneous velocity and concentration measurements of buoyant jet discharges with combined DPIV and PLIF. 2nd International Symposium on Environmental Hydraulics, Hong Kong, pp. 211-216.
- Lubbers, C.L., Brethouwer, G. & Boersma, B.J. 2000 Simulation of the mixing of a passive scalar in a round turbulent jet. *In preparation*.
- Panchapakesan, N.R. & Lumley, J.L. 1993 Turbulence measurements in axisymmetric jets of air and helium. Part 1. Air jet. *J. Fluid Mech.* **246**, 197-223.
- Papanicolaou, P.N. & List, E.J. 1988 Investigation of round vertical turbulent buoyant jets. *J. Fluid Mech.* **195**, 341-391.
- Walker, D.A. 1987 A fluorescent technique for measurement of concentration in mixing liquids. *J. Phys.E. Sci. Instrum.* **20**, 217-224.
- Webster, D.R., Roberts, P.J.W. & Ra'ad, L. 2000 Simultaneous DPTV/PLIF measurements of a turbulent jet. Submitted to *Exp. Fluids*. (Also 3rd International Workshop on Particle Image Velocimetry, Santa Barbara, California, 1999)
- Westerweel, J. 1993 *Digital Particle Image Velocimetry – Theory and Application*. Delft University Press.
- Wynanski, I. & Fiedler, H. 1969 Some measurements in the self-preserving jet. *J. Fluid Mech.* **38-3**, 577-612.